

A Record-High Cryogenic Magnetocaloric Effect Discovered in EuCl₂ Compound

Bingjie Wang,[◆] Xinyang Liu,[◆] Fengxia Hu,^{*} Jian-tao Wang, Junsen Xiang, Peijie Sun, Jing Wang,^{*} Jirong Sun, Tongyun Zhao, Zhaojun Mo, Jun Shen, Yunzhong Chen, Qingzhen Huang, and Baogen Shen^{*}



Cite This: *J. Am. Chem. Soc.* 2024, 146, 35016–35022



Read Online

ACCESS |



Metrics & More



Article Recommendations



Supporting Information

ABSTRACT: Adiabatic demagnetization refrigeration (ADR) based on the magnetocaloric effect (MCE) is a promising technique to achieve cryogenic temperature. However, magnetic entropy change (ΔS_M), the driving force of ADR, remains far below theoretical $-\Delta S_M = nR \ln(2J + 1)/M_W$ for most magnetic refrigerants. Here, we report giant MCE in orthorhombic EuCl₂, where a ferromagnetic ground state with excellent single-ion behavior of Eu²⁺ and free spins has been demonstrated by combining *ab initio* calculations with Brillouin function analysis and magnetic measurements. Consequently, a record-high $-\Delta S_M \sim 74.6 \text{ J}\cdot\text{kg}^{-1}\cdot\text{K}^{-1}$ (1.8 K) at 5 T was experimentally achieved, approaching 96% of the theoretical limit ($77.5 \text{ J}\cdot\text{kg}^{-1}\cdot\text{K}^{-1}$). At a lower field of 1 T, EuCl₂ also achieves the highest-ever record of $-\Delta S_M \sim 36.8 \text{ J}\cdot\text{kg}^{-1}\cdot\text{K}^{-1}$. Further, direct quasi-adiabatic demagnetization measurements demonstrate that its large $-\Delta S_M$ allows EuCl₂ to maintain a long holding time at sub-Kelvin temperature ($\sim 346 \text{ mK}$), surpassing all previously reported materials. These superior magnetocaloric performances position EuCl₂ as an attractive cryogenic refrigerant.

Cryogenic refrigeration techniques are increasingly vital due to helium shortage, especially given their extensive use in space applications, quantum technology, and other frontier scientific research fields.^{1–3} Adiabatic demagnetization refrigeration (ADR), based on the magnetocaloric effect (MCE), presents a promising method for achieving sub-Kelvin temperatures without using the rare ³He–⁴He.^{4,5} Considering that the magnetic entropy changes (ΔS_M) of magnetic refrigerants act as the driving force of ADR, the exploitation of materials with large ΔS_M is not only important for ADR but also for the design of an ADR system.⁶ To obtain magnetic refrigerants with a large MCE, various attempts have been made on Gd-based materials, and significant MCE has been achieved at cryogenic temperatures by utilizing large ground-state spin ($J = S = 7/2$, $L = 0$) of Gd³⁺ ions and magnetic isotropy,^{7–18} where J , S , and L denote total, spin, and orbital angular momentum quantum number, respectively. However, under low magnetic fields, the achieved ΔS_M of most Gd-based materials still remains far below the theoretical $-\Delta S_M = nR \ln(2J + 1)/M_W$, where n represents the number of uncoupled spins, R is the gas constant, and M_W represents the formula weight of the compound. Generally, to make the ΔS_M approach the theoretical limit, following characteristics are required:^{19–21} (1) large J , i.e., large saturation magnetic moment; (2) weak magnetic anisotropy, particularly those with $L = 0$, allowing for easier alignment when subjected to external magnetic fields; (3) high magnetic density M_R/M_W , where M_R represents weight of magnetic elements and M_W represents compound weight; (4) weak magnetic interactions and near single-ion behavior, ensuring that materials behave in a manner where individual ions respond almost independently to

magnetic fields; (5) low ordering temperature, which is beneficial to MCE.²²

Since Eu²⁺ ions share the same $J = S = 7/2$, $L = 0$, and magnetic isotropy as Gd³⁺ ions, divalent europium compounds have also attracted attention in exploring cryogenic magnetocaloric materials. Some materials, such as EuB₄O₇²³ and EuB₂O₄,²⁴ have been discovered showing large MCE around 1.3 K. However, the relatively low magnetic density and complex interactions between Eu²⁺ ions due to coordination ligands make their ΔS_M far below the theoretical limit. Europium dihalides (EuX₂, X = F, Cl, Br, and I) with simple ligands come into our sights due to their high magnetic ion densities ($M_{Eu}/M_W = 80\%$, 68%, 49%, 37%, respectively) and high theoretical ΔS_M , which approaches 91.0, 77.5, 55.4, and 42.6 $\text{J}\cdot\text{kg}^{-1}\cdot\text{K}^{-1}$ from $-\Delta S_M = nR \ln(2S + 1)/M_W$, for X = F, Cl, Br, and I, respectively.

In this work, we focus on EuCl₂ since EuF₂ exhibits robust antiferromagnetic coupling insensitive to magnetic fields. Ultrahigh purity (99.99%) polycrystalline EuCl₂ powder was purchased from Aladdin. PXRD and Rietveld refinements (SI-2) reveal that EuCl₂ crystallizes in an orthorhombic structure with space group *Pnma*. Each Eu atom coordinates with nine Cl atoms, and the Eu–Cl distances vary in the range of 2.907–3.431 Å, leading to a slightly distorted structure akin to a tricapped trigonal prism, as shown in Figure 1a,b. Cl atoms

Received: September 8, 2024

Revised: November 27, 2024

Accepted: November 27, 2024

Published: December 4, 2024



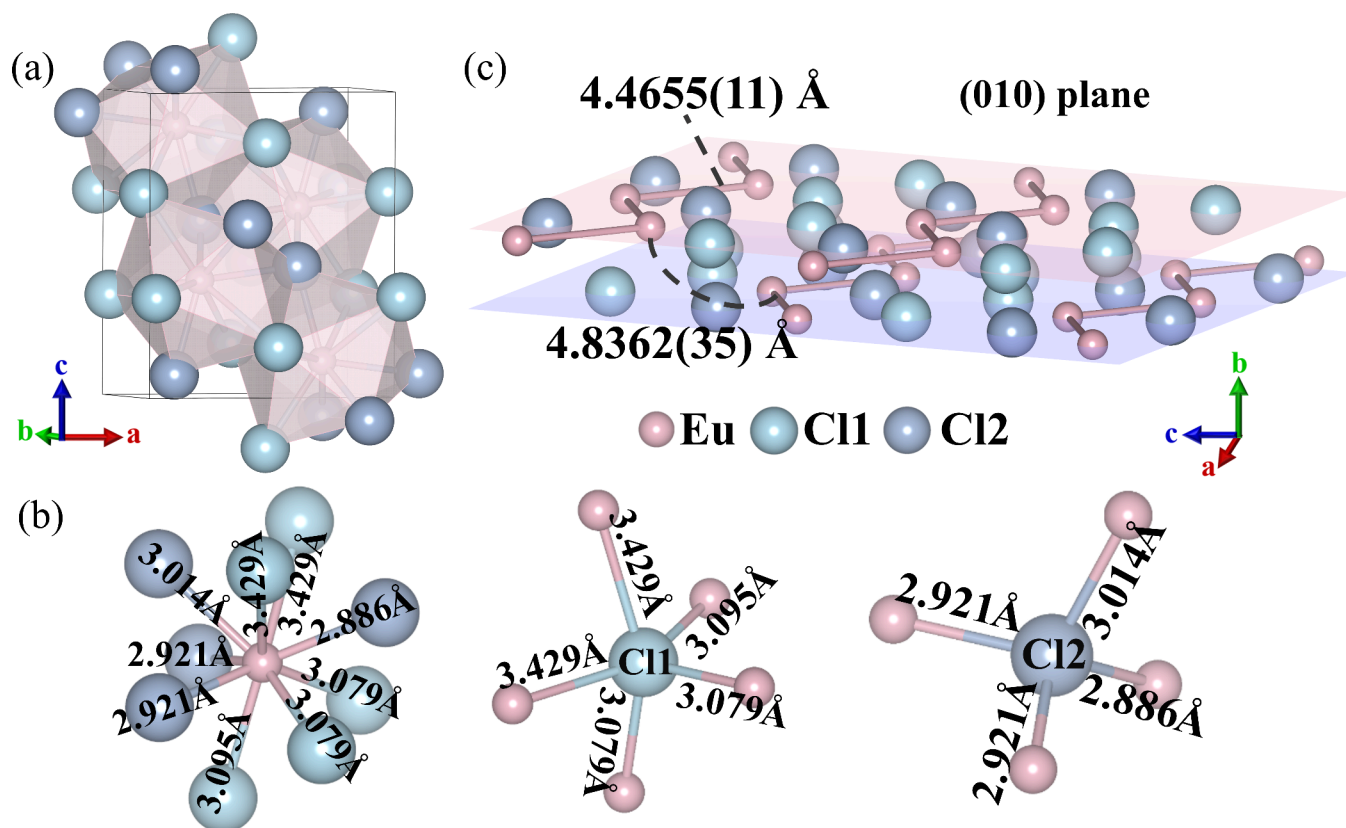


Figure 1. Crystallographic structure for EuCl_2 . (a) Each Eu atom coordinates with nine Cl atoms. (b) Nearest neighbor elemental environments for Eu, Cl1, and Cl2. (c) Two (010) planes along the b axis.

occupy two inequivalent sites: at the Cl1 site, each Cl is bonded to five equivalent Eu atoms, while at the Cl2 site, each Cl is connected to four Eu atoms, forming edge- and corner-sharing ClEu_4 tetrahedra. Figure 1c depicts two (010) planes along the b -axis. Eu atoms form Eu–Eu 1D chains in the (010) plane, where the shortest Eu–Eu distance is 4.4655(11) Å, while between the (010) planes, the Eu–Eu distance is 4.8362(35) Å. Notably, the shortest distance between Eu^{2+} ions in EuCl_2 is larger than that reported in other Eu^{2+} MCE compounds, such as 4.24 Å in EuB_4O_7 ²³ and 3.84 Å in EuB_2O_4 .²⁴ The larger distances among Eu^{2+} ions favor weak Heisenberg interactions and hence promote single-ion behavior.

To know the nature of the magnetic ground state of EuCl_2 , magnetic measurements and total energy calculations of different spin configurations were conducted. Measurements above 1.8 K were collected on the MPMS-3 system, while ultralow temperature measurements from 1.8 to 0.4 K were conducted by ^3He -insert in the MPMS-3 system. Figure 2a plots the temperature-dependent magnetization (M - T) under both zero-field cooling (ZFC) and field cooling (FC) with an applied magnetic field of 0.01 T from 0.4 to 300 K. Figure 2b shows the temperature-dependent reciprocal susceptibility ($1/\chi = H/M$). From the Curie–Weiss fitting $\chi^{-1} = 3k_{\text{B}}(T - \theta_{\text{CW}})/N(\mu_{\text{B}}\mu_{\text{eff}})^2$, where k_{B} is the Boltzmann constant and N represents Avogadro's number, the determined effective magnetic moment μ_{eff} and paramagnetic Curie temperature θ_{CW} are 7.62 μ_{B} and 1.30 K, respectively. Note that the theoretical moment of free Eu^{2+} ion ($J = S = 7/2, L = 0$) is 7.94 μ_{B} based on $g_{\text{J}}\sqrt{J(J+1)}$, where $g_{\text{J}} = 2$. The experimental value

(7.62 μ_{B}) from the Curie–Weiss law closely matches the theoretical value, and the positive θ_{CW} (1.30 K) reveals that ferromagnetic (FM) interaction is dominant in EuCl_2 . To convince the FM nature of magnetic ground state, we further computed the total energy of four spin configurations by DFT calculations, e.g., linear FM, A-type, C-type, and G-type antiferromagnetic (AFM) alignments; see Figure 2c–f, the calculated total energy is -85.733528 , -85.730356 , -85.730425 , and -85.729547 eV/f.u., respectively. The linear FM configuration exhibits the lowest energy for EuCl_2 . Further, the density of states (DOS) was calculated to investigate the electronic structures of EuCl_2 . Figure 2g gives the total DOS (TDOS) and partial DOS (PDOS) for the Eu-4f and Cl bands. For Eu-4f bands, the spin-up states situated below the Fermi level (E_{F}) exhibit a sharp peak at around -0.35 eV, while the spin-down bands situate far above E_{F} . On the other hand, the Cl bands almost equally populate without bias and without any hybridization with Eu bands, which contribute negligibly to the TDOS and total moment. These behaviors underscore the high localization of the Eu-4f electrons. Moreover, the TDOS at E_{F} is negligible, which limits electron mobility. All these reveal the band origin of FM properties and imply the near single-ion behavior of Eu^{2+} in EuCl_2 is due to the negligible coupling between Eu and Cl.

Electron localization function (ELF) is a powerful means of quantitatively characterizing electronic localization in space.^{25–27} The calculated ELF map in the (010) plane is given in Figure 3a, from which the extracted ELF values between the nearest-neighbor Eu–Cl (Eu–Cl1 and Eu–Cl2) are plotted in Figure 3b. Generally, ELF values changing from 0 to 1 correspond to electrons from total delocalization to

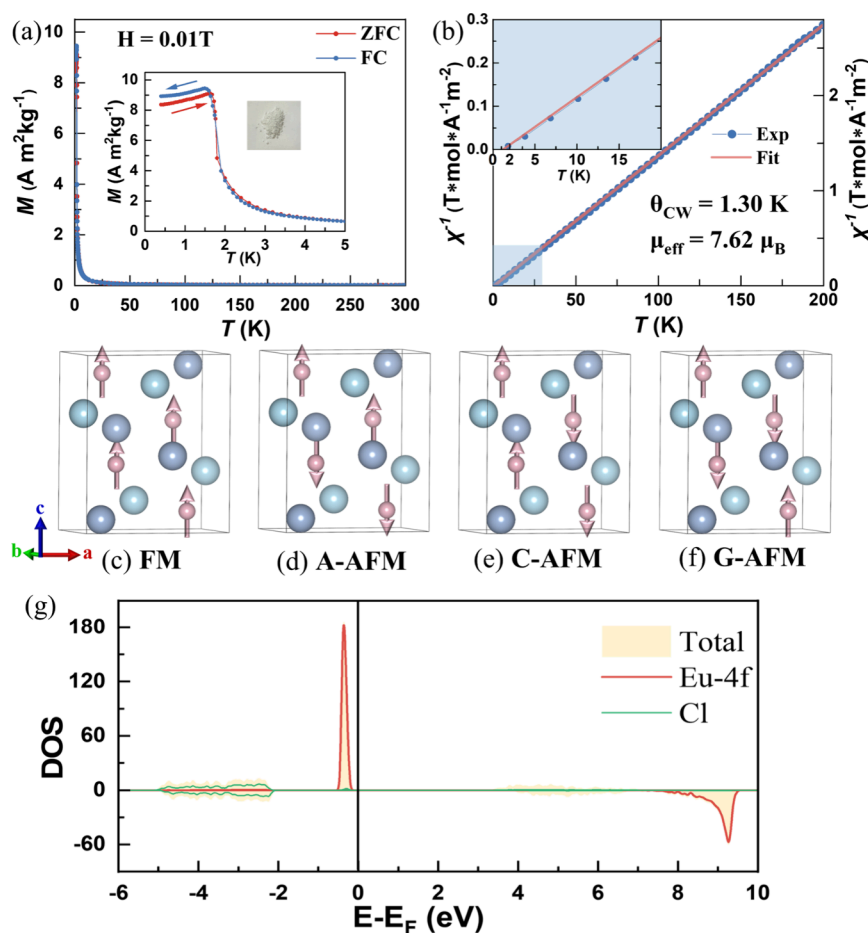


Figure 2. (a) M - T curve of ZFC and FC branches from 0.4 to 300 K at $H = 0.01 \text{ T}$. The inset gives the zoom-in curves and topography of EuCl_2 powder. (b) ZFC inverse susceptibility χ^{-1} fitted to the Curie–Weiss law. The inset gives the enlarged region approaching zero. (c–f) Four magnetic configurations: FM, A-type, C-type, and G-type AFM; (g) total and partial DOS of Eu-4f and Cl.

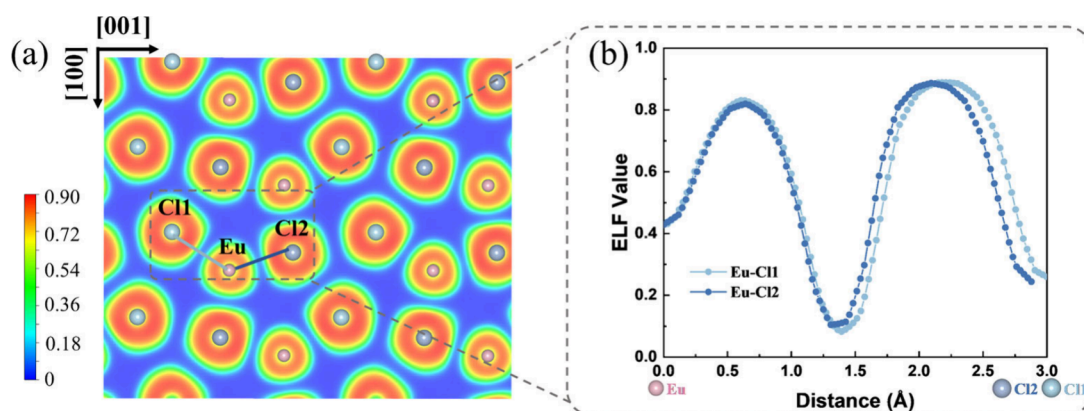


Figure 3. (a) ELF on (010) plane. (b) Line profile of the ELF value between nearest-neighbor Eu and Cl1 or Cl2.

complete localization. The large ELF values (>0.8) around Eu and Cl indicate highly localized electron distribution around either Eu or Cl. The subtle different sites of Cl1 and Cl2 can also be identified from Figure 3b, but their ELF values remain nearly the same, both slightly higher than that of Eu due to the large electronegativity of Cl. In contrast, in the middle region between Eu and Cl, the ELF approaches zero (<0.1) with negligible electron share, evidencing the magnetic behavior of Eu^{2+} ions close to magnetic single-ion.

To further confirm the nearly free spin behavior of Eu^{2+} ions in EuCl_2 , the prediction of the free Heisenberg spin model was compared with experimental data. This model provides a robust framework for describing magnetization M , under an applied field H and temperature T .^{28,29} The magnetization is expressed as follows (see SI-5):

$$M = M_0 B_J(x) \quad (1)$$

where the Brillouin function $B_J(x)$ is defined as:

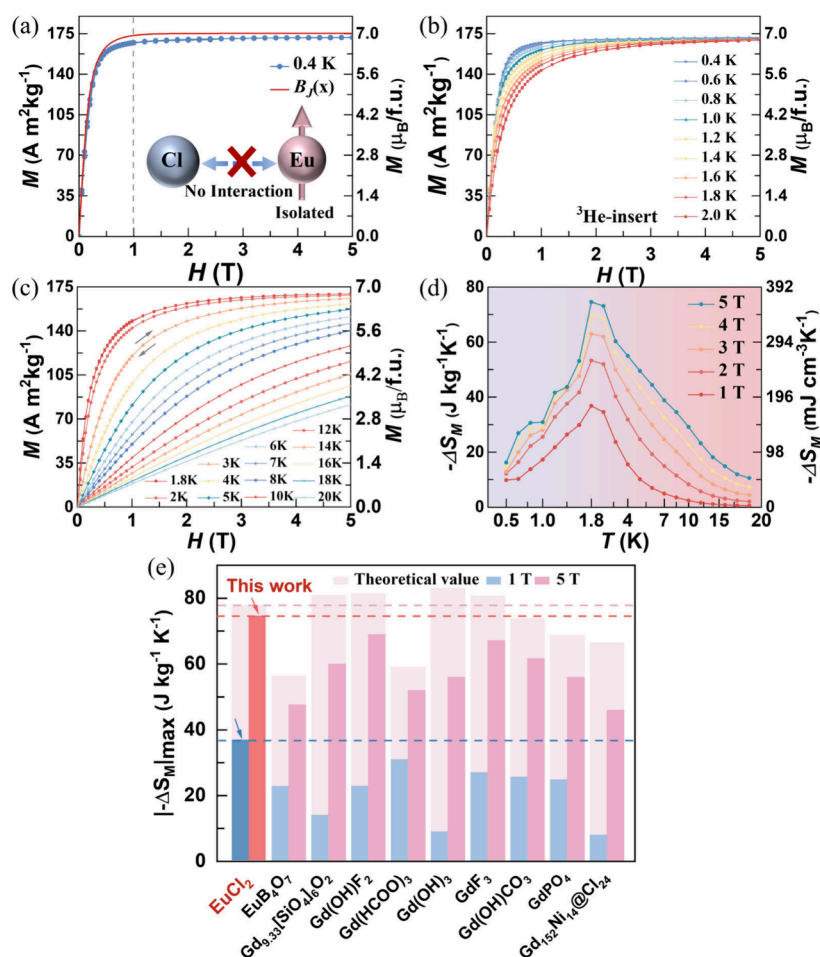


Figure 4. (a) Measured M - H curve and the Brillouin-like free spins $B_j(x)$ at $T = 0.4$ K. Inset depicts the sketch of Eu^{2+} free spins. M - H curves (b) from 0.4 to 2 K and (c) from 1.8 to 20 K. (d) $-\Delta S_M$ from 0.4 to 20 K. (e) Comparison of $|\Delta S_M|_{\text{max}}$ for EuCl_2 with other cryogenic magnetocaloric materials^{11,13,15,16,18,23,30–32} at $H = 1$ T (blue) and $H = 5$ T (pink); light pink denotes theoretical value from $-\Delta S_M = nR \ln(2S + 1)/M_W$.

$$B_j(x) = \frac{1}{2J} \left[(2J + 1) \coth \frac{2J + 1}{2J} x - \coth \frac{x}{2J} \right] \quad (2)$$

This function describes the magnetization behavior of an ideal paramagnet, where spin interactions are minimal. The Brillouin function for one magnetically uncoupled Eu^{2+} ion with $S = 7/2$ and $g_j = 2$ at 0.4 K was calculated, as shown in Figure 4a, which is comparatively plotted with the measured M - H curve at 0.4 K of EuCl_2 . It is evident that similar to the theoretical curve, the measured magnetization increases sharply at low fields, reaching approximately 97.4% saturation at 1 T. The good match with the Brillouin function supports the free spin behaviors of Eu^{2+} ions. The measured saturation magnetic moment is slightly lower than but approaches about 98% of the classical theoretical saturation value $\mu_{jz} = g_j \mu_B$ ($7 \mu_B/\text{f.u.}$), which can be attributed to a small amount of EuOCl impurities by PXRD.

The near single-ion behavior and weak interactions of Eu^{2+} ions in FM EuCl_2 make spins easily align with applied external fields; hence, a significantly high MCE with ΔS_M approaching the theoretical limit is expected considering the high magnetic moment of Eu^{2+} ions.

We characterized the magnetocaloric properties of EuCl_2 by magnetic measurements (Figure 4b,c). Our studies on Arrott plots, scaling analysis, and the n -exponent collectively indicate a second-order phase transition in EuCl_2 , see details in SI-6.

The maximum $-\Delta S_M$ from Maxwell relation reaches $74.6 \text{ J} \cdot \text{kg}^{-1} \cdot \text{K}^{-1}$ at $T = 1.8$ K and $H = 5$ T, approximately 96% of the theoretical value of $77.5 \text{ J} \cdot \text{kg}^{-1} \cdot \text{K}^{-1}$. At a lower field $H = 1$ T, the $-\Delta S_M$ achieves up to $36.8 \text{ J} \cdot \text{kg}^{-1} \cdot \text{K}^{-1}$ at $T = 1.8$ K (Figure 4d). Figure 4e compares the magnetocaloric performance of EuCl_2 with some excellent Gd^{3+} - and Eu^{2+} -based cryogenic refrigerants,^{11,13,15,16,18,23,30–32} where the experimental $|\Delta S_M|_{\text{max}}$ at 1 T and 5 T along with theoretical $-\Delta S_M$ from $-\Delta S_M = nR \ln(2S + 1)/M_W$ are given. Although the theoretical limit for EuCl_2 is not the largest, the experimental $-\Delta S_M$ at 5 T exceeds that of all others and approaches its theoretical limit more closely than anyone else (see SI-7). More attractively, due to the nearly free spin behaviors of Eu^{2+} ions in EuCl_2 and the driven easy saturation (Figure 4a), the $-\Delta S_M \sim 36.8 \text{ J} \cdot \text{kg}^{-1} \cdot \text{K}^{-1}$ at a low field of 1 T also surpasses that of all other materials, and, in particular, it is approximately twice as high as that of commercial cryogenic refrigerant $\text{Gd}_3\text{Ga}_5\text{O}_{12}$ (GGG) with $-\Delta S_M \sim 21 \text{ J} \cdot \text{kg}^{-1} \cdot \text{K}^{-1}$ at 2 times field (2 T).¹⁷ The significant MCE positions EuCl_2 as a promising candidate for cryogenic refrigerants in practical applications.

Further, quasi-adiabatic demagnetization measurements were conducted to investigate the cooling performance as a cryogenic refrigerant. The lowest achievable temperature is a key indicator of the ADR material performance. Holding time at low temperatures is another more critical parameter for evaluating the actual performance of an ADR system, as it

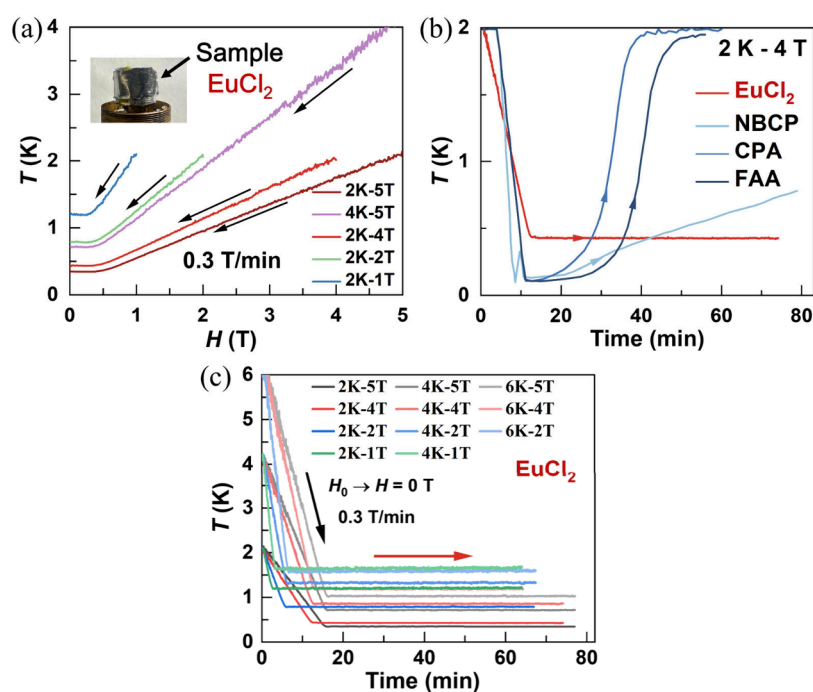


Figure 5. (a) Quasi-adiabatic demagnetization cooling curves of EuCl₂ at different initial conditions ((T₀, H₀) = (2 K, 1 T), (2 K, 2 T), (2 K, 4 T), (2 K, 5 T), (4 K, 5 T)). Inset gives the sample setup. (b) Comparison of the holding time of EuCl₂ with Na₂BaCo(PO₄)₂ (NBCP), CrK(SO₄)₂·12H₂O (CPA), and Fe(SO₄)₂(NH₄)₂·6H₂O (FAA)³⁶ under same initial condition T₀ = 2 K, H₀ = 4 T. Adapted with permission from ref [36]. Copyright [2024] [Springer Nature]. (c) Holding time of EuCl₂ under other initial conditions. Arrows indicate the direction of demagnetizing field and time.

determines how long the system can operate effectively without the need to restart the cooling cycle, which is important for continuous or long-duration applications.^{23,33–35} Using the homemade device on PPMS,³⁶ the demagnetization cooling was measured. Figure 5a illustrates the demagnetization curves under various initial conditions (T₀, H₀). At initial condition (2 K, 5 T), EuCl₂ reaches the lowest temperature of 346 mK, and under (2 K, 4 T), it achieves the lowest temperature of 428 mK. Figure 5b depicts the holding time for EuCl₂ in comparison with other famous cryogenic refrigerants CPA, FAA, and NBCP.³⁶ Despite heat leakage, the holding time of EuCl₂ at any initial conditions is over an hour (see Figure 5c), significantly longer than any other materials under the same working condition. Although the frustrated quantum spin liquid materials can bring a lower temperature, the temperature quickly rises due to small $-\Delta S_M$.³⁷ The long holding time at the lowest achievable temperature is mainly attributed to the large $-\Delta S_M$.^{23,38–40} Materials with larger $-\Delta S_M$ values can store more magnetic entropy during demagnetization. This means that the material can better maintain the low-temperature state and reduce the temperature increase in the absence of external intervention, thus prolonging the holding time.

In summary, our detailed studies on EuCl₂ have uncovered weak FM couplings and the near single-ion behavior of Eu²⁺ ions, which are pivotal for its superior magnetocaloric performances. The achieved $-\Delta S_M \sim 74.6 \text{ J}\cdot\text{kg}^{-1}\cdot\text{K}^{-1}$ at 5 T and 1.8 K approaches the theoretical limit with a record-high ratio of 96%, surpassing all previously known cryogenic refrigerants. Furthermore, $-\Delta S_M \sim 36.8 \text{ J}\cdot\text{kg}^{-1}\cdot\text{K}^{-1}$ at 1 T is also the largest at the same magnetic field. Most importantly, direct quasi-adiabatic demagnetization measurements reveal that EuCl₂ with large $-\Delta S_M$ achieves a long holding time at

$\sim 346 \text{ mK}$, which exceeds all previously reported materials. These groundbreaking results establish EuCl₂ as a highly promising material for ADR applications.

■ ASSOCIATED CONTENT

Supporting Information

The Supporting Information is available free of charge at <https://pubs.acs.org/doi/10.1021/jacs.4c12441>.

Experimental details, computational methods, and supplementary figures and tables (PDF)

■ AUTHOR INFORMATION

Corresponding Authors

Fengxia Hu – Beijing National Laboratory for Condensed Matter Physics, Institute of Physics, Chinese Academy of Sciences, Beijing 100190, People's Republic of China; School of Physical Sciences, University of Chinese Academy of Sciences, Beijing 101408, People's Republic of China; Songshan Lake Materials Laboratory, Dongguan, Guangdong 523808, People's Republic of China; Email: fxhu@iphy.ac.cn

Jing Wang – Beijing National Laboratory for Condensed Matter Physics, Institute of Physics, Chinese Academy of Sciences, Beijing 100190, People's Republic of China; School of Physical Sciences, University of Chinese Academy of Sciences, Beijing 101408, People's Republic of China; orcid.org/0000-0001-5458-6711; Email: wangjing@iphy.ac.cn

Baogen Shen – Beijing National Laboratory for Condensed Matter Physics, Institute of Physics, Chinese Academy of Sciences, Beijing 100190, People's Republic of China; School of Physical Sciences, University of Chinese Academy of Sciences, Beijing 101408, People's Republic of China;

Ganjiang Innovation Academy, Chinese Academy of Sciences, Ganzhou, Jiangxi 341000, People's Republic of China; Ningbo Institute of Materials Technology & Engineering, Chinese Academy of Sciences, Ningbo, Zhejiang 315201, People's Republic of China; orcid.org/0000-0003-4819-1806; Email: shenbg@diphy.ac.cn

National Laboratory for Condensed Matter Physics, Institute of Physics, Chinese Academy of Sciences, Beijing 100190, People's Republic of China

Complete contact information is available at: <https://pubs.acs.org/10.1021/jacs.4c12441>

Authors

Bingjie Wang – Beijing National Laboratory for Condensed Matter Physics, Institute of Physics, Chinese Academy of Sciences, Beijing 100190, People's Republic of China; School of Physical Sciences, University of Chinese Academy of Sciences, Beijing 101408, People's Republic of China

Xinyang Liu – Beijing National Laboratory for Condensed Matter Physics, Institute of Physics, Chinese Academy of Sciences, Beijing 100190, People's Republic of China; School of Physics, Beihang University, Beijing 100191, People's Republic of China

Jian-tao Wang – Beijing National Laboratory for Condensed Matter Physics, Institute of Physics, Chinese Academy of Sciences, Beijing 100190, People's Republic of China; School of Physical Sciences, University of Chinese Academy of Sciences, Beijing 101408, People's Republic of China; Songshan Lake Materials Laboratory, Dongguan, Guangdong 523808, People's Republic of China; orcid.org/0000-0002-0786-1212

Junsen Xiang – Beijing National Laboratory for Condensed Matter Physics, Institute of Physics, Chinese Academy of Sciences, Beijing 100190, People's Republic of China; School of Physical Sciences, University of Chinese Academy of Sciences, Beijing 101408, People's Republic of China

Peijie Sun – Beijing National Laboratory for Condensed Matter Physics, Institute of Physics, Chinese Academy of Sciences, Beijing 100190, People's Republic of China; School of Physical Sciences, University of Chinese Academy of Sciences, Beijing 101408, People's Republic of China

Jirong Sun – Beijing National Laboratory for Condensed Matter Physics, Institute of Physics, Chinese Academy of Sciences, Beijing 100190, People's Republic of China; School of Physical Sciences, University of Chinese Academy of Sciences, Beijing 101408, People's Republic of China; Songshan Lake Materials Laboratory, Dongguan, Guangdong 523808, People's Republic of China; orcid.org/0000-0003-4531-4794

Tongyun Zhao – Beijing National Laboratory for Condensed Matter Physics, Institute of Physics, Chinese Academy of Sciences, Beijing 100190, People's Republic of China; Ganjiang Innovation Academy, Chinese Academy of Sciences, Ganzhou, Jiangxi 341000, People's Republic of China

Zhaojun Mo – Ganjiang Innovation Academy, Chinese Academy of Sciences, Ganzhou, Jiangxi 341000, People's Republic of China; orcid.org/0000-0001-5183-4302

Jun Shen – Department of Energy and Power Engineering, School of Mechanical Engineering, Beijing Institute of Technology, Beijing 100081, People's Republic of China

Yunzhong Chen – Beijing National Laboratory for Condensed Matter Physics, Institute of Physics, Chinese Academy of Sciences, Beijing 100190, People's Republic of China; School of Physical Sciences, University of Chinese Academy of Sciences, Beijing 101408, People's Republic of China; orcid.org/0000-0001-8368-5823

Qingzhen Huang – Spallation Neutron Source Science Center, Dongguan 523803, People's Republic of China; Beijing

Author Contributions

◆ B.-J. W. and X.-Y. L. contributed equally.

Notes

The authors declare no competing financial interest.

ACKNOWLEDGMENTS

This work was supported by the Science Center of the National Science Foundation of China (52088101), the National Key Research and Development Program of China (2021YFB3501202, 2019YFA0704900, 2023YFA1406003, 2020YFA0711500, 2021YFA1400300), the National Natural Sciences Foundation of China (92263202, U23A20550, 22361132534), the Strategic Priority Research Program B (XDB33030200) of Chinese Academy of Sciences (CAS), and the Synergetic Extreme Condition User Facility (SECUF).

REFERENCES

- (1) McClintock, P. V. E. Will Detente Kill Millikelvin Research? *Nature* **1978**, 276 (5684), 117.
- (2) Stone, R. Researchers Rise to Challenge of Replacing Helium-3. *Science* **2016**, 353 (6294), 15–16.
- (3) Cho, A. Helium-3 Shortage Could Put Freeze On Low-Temperature Research. *Science* **2009**, 326 (5954), 778–779.
- (4) Franco, V.; Blázquez, J. S.; Ipus, J. J.; Law, J. Y.; Moreno-Ramírez, L. M.; Conde, A. Magnetocaloric Effect: From Materials Research to Refrigeration Devices. *Prog. Mater. Sci.* **2018**, 93, 112–232.
- (5) Shen, B. G.; Sun, J. R.; Hu, F. X.; Zhang, H. W.; Cheng, Z. H. Recent Progress in Exploring Magnetocaloric Materials. *Adv. Mater.* **2009**, 21 (45), 4545–4564.
- (6) Fukuda, H.; Ueda, S.; Arai, R.; Li, J.; Saito, A. T.; Nakagome, H.; Numazawa, T. Properties of a Two Stage Adiabatic Demagnetization Refrigerator. *IOP Conf. Ser.: Mater. Sci. Eng.* **2015**, 101, No. 012047.
- (7) Tziotzi, T. G.; Gracia, D.; Dalgarno, S. J.; Schnack, J.; Evangelisti, M.; Brechin, E. K.; Milios, C. J. A {Gd₁₂Na₆} Molecular Quadruple-Wheel with a Record Magnetocaloric Effect at Low Magnetic Fields and Temperatures. *J. Am. Chem. Soc.* **2023**, 145 (14), 7743–7747.
- (8) Zheng, X.-Y.; Jiang, Y.-H.; Zhuang, G.-L.; Liu, D.-P.; Liao, H.-G.; Kong, X.-J.; Long, L.-S.; Zheng, L.-S. A Gigantic Molecular Wheel of {Gd₁₄₀}: A New Member of the Molecular Wheel Family. *J. Am. Chem. Soc.* **2017**, 139 (50), 18178–18181.
- (9) Luo, X.-M.; Hu, Z.-B.; Lin, Q.; Cheng, W.; Cao, J.-P.; Cui, C.-H.; Mei, H.; Song, Y.; Xu, Y. Exploring the Performance Improvement of Magnetocaloric Effect Based Gd-Exclusive Cluster Gd₆₀. *J. Am. Chem. Soc.* **2018**, 140 (36), 11219–11222.
- (10) Xu, Q.-F.; Liu, B.-L.; Ye, M.-Y.; Long, L.-S.; Zheng, L.-S. Magnetocaloric Effect and Thermal Conductivity of a 3D Coordination Polymer of [Gd(HCOO)(C₂O₄)]_n. *Inorg. Chem.* **2021**, 60 (13), 9259–9262.
- (11) Yang, Y.; Zhang, Q.-C.; Pan, Y.-Y.; Long, L.-S.; Zheng, L.-S. Magnetocaloric Effect and Thermal Conductivity of Gd(OH)₃ and Gd₂O(OH)₄(H₂O)₂. *Chem. Commun.* **2015**, 51 (34), 7317–7320.
- (12) Sibille, R.; Didelot, E.; Mazet, T.; Malaman, B.; François, M. Magnetocaloric Effect in Gadolinium-Oxalate Framework Gd₂(C₂O₄)₃(H₂O)₆·(0.6H₂O). *APL Mater.* **2014**, 2 (12), No. 124402.
- (13) Chen, Y.-C.; Qin, L.; Meng, Z.-S.; Yang, D.-F.; Wu, C.; Fu, Z.; Zheng, Y.-Z.; Liu, J.-L.; Tarasenko, R.; Orendáč, M.; Prokleška, J.;

- Sechovský, V.; Tong, M.-L. Study of a Magnetic-Cooling Material $\text{Gd}(\text{OH})\text{CO}_3$. *J. Mater. Chem. A* **2014**, *2* (25), 9851–9858.
- (14) Hatscher, S. T.; Urland, W. Unexpected Appearance of Molecular Ferromagnetism in the Ordinary Acetate $[\text{Gd}(\text{OAc})_3(\text{H}_2\text{O})_{22}] \cdot 4\text{H}_2\text{O}$. *Angew. Chem., Int. Ed.* **2003**, *42* (25), 2862–2864.
- (15) Yang, Z. W.; Zhang, J.; Liu, B.; Zhang, X.; Lu, D.; Zhao, H.; Pi, M.; Cui, H.; Zeng, Y.; Pan, Z.; Shen, Y.; Li, S.; Long, Y. Exceptional Magnetocaloric Responses in a Gadolinium Silicate with Strongly Correlated Spin Disorder for Sub-Kelvin Magnetic Cooling. *Adv. Sci.* **2024**, *11*, No. 2306842.
- (16) Xu, N.; Chen, W.; Ding, Y.; Zheng, Z. A Cubic Tinkertoy-like Heterometallic Cluster with a Record Magnetocaloric Effect. *J. Am. Chem. Soc.* **2024**, *146* (14), 9506–9511.
- (17) Daudin, B.; Lagnier, R.; Salce, B. Thermodynamic Properties of the Gadolinium Gallium Garnet, $\text{Gd}_3\text{Ga}_5\text{O}_{12}$, between 0.05 and 25 K. *J. Magn. Magn. Mater.* **1982**, *27* (3), 315–322.
- (18) Palacios, E.; Rodríguez-Velamazán, J. A.; Evangelisti, M.; McIntyre, G. J.; Lorusso, G.; Visser, D.; De Jongh, L. J.; Boatner, L. A. Magnetic Structure and Magnetocalorics of GdPO_4 . *Phys. Rev. B* **2014**, *90* (21), No. 214423.
- (19) Liu, J.-L.; Chen, Y.-C.; Guo, F.-S.; Tong, M.-L. Recent Advances in the Design of Magnetic Molecules for Use as Cryogenic Magnetic Coolants. *Coord. Chem. Rev.* **2014**, *281*, 26–49.
- (20) Liu, S.-J.; Han, S.-D.; Zhao, J.-P.; Xu, J.; Bu, X.-H. In-Situ Synthesis of Molecular Magnetorefrigerant Materials. *Coord. Chem. Rev.* **2019**, *394*, 39–52.
- (21) Zheng, Y.-Z.; Zhou, G.-J.; Zheng, Z.; Winpenny, R. E. P. Molecule-Based Magnetic Coolers. *Chem. Soc. Rev.* **2014**, *43* (5), 1462–1475.
- (22) Liu, W.; Gottschall, T.; Scheibel, F.; Bykov, E.; Aubert, A.; Fortunato, N.; Beckmann, B.; Döring, A. M.; Zhang, H.; Skokov, K.; Gutfleisch, O. A matter of performance and criticality: a review of rare-earth-based magnetocaloric intermetallic compounds for hydrogen liquefaction. *J. Alloys Compd.* **2024**, *995*, No. 174612.
- (23) Wang, Y.; Xiang, J.; Zhang, L.; Gong, J.; Li, W.; Mo, Z.; Shen, J. Giant Low-Field Cryogenic Magnetocaloric Effect in a Polycrystalline Eu_4O_7 Compound. *J. Am. Chem. Soc.* **2024**, *146* (5), 3315–3322.
- (24) Wang, Y.; Liu, Q.; Tian, L.; Hao, Z.; Zhang, L.; Fu, Q.; Zhao, J.; Mo, Z. A Cryogenic Magnetic Refrigerant: Magnetocaloric Study of Eu_2O_4 Compound. *J. Alloys Compd.* **2024**, *995*, No. 174753.
- (25) Becke, A. D.; Edgecombe, K. E. A Simple Measure of Electron Localization in Atomic and Molecular Systems. *J. Chem. Phys.* **1990**, *92* (9), 5397–5403.
- (26) Silvi, B.; Savin, A. Classification of Chemical Bonds Based on Topological Analysis of Electron Localization Functions. *Nature* **1994**, *371* (6499), 683–686.
- (27) Savin, A.; Jepsen, O.; Flad, J.; Andersen, O. K.; Preuss, H.; Von Schnering, H. G. Electron Localization in Solid-State Structures of the Elements: The Diamond Structure. *Angew. Chem., Int. Ed. Engl.* **1992**, *31* (2), 187–188.
- (28) Oyeka, E. E.; Winiarski, M. J.; Świątek, H.; Balliew, W.; McMillen, C. D.; Liang, M.; Sorolla, M.; Tran, T. T. $\text{Ln}_2(\text{SeO}_3)_2(\text{SO}_4)(\text{H}_2\text{O})_2$ ($\text{Ln} = \text{Sm}, \text{Dy}, \text{Yb}$): A Mixed-Ligand Pathway to New Lanthanide(III) Multifunctional Materials Featuring Nonlinear Optical and Magnetic Anisotropy Properties. *Angew. Chem. Int. Ed.* **2022**, *61* (48), No. e202213499.
- (29) Koskela, E. C.; Liu, C.; Mukherjee, P.; Kelly, N. D.; Dutton, S. E. Free-Spin Dominated Magnetocaloric Effect in Dense Gd^{3+} Double Perovskites. *Chem. Mater.* **2022**, *34* (7), 3440–3450.
- (30) Xu, Q.; Liu, B.; Ye, M.; Zhuang, G.; Long, L.; Zheng, L. $\text{Gd}(\text{OH})\text{F}_2$: A Promising Cryogenic Magnetic Refrigerant. *J. Am. Chem. Soc.* **2022**, *144* (30), 13787–13793.
- (31) Lorusso, G.; Sharples, J. W.; Palacios, E.; Roubeau, O.; Brechin, E. K.; Sessoli, R.; Rossin, A.; Tuna, F.; McInnes, E. J. L.; Collison, D.; Evangelisti, M. A Dense Metal–Organic Framework for Enhanced Magnetic Refrigeration. *Adv. Mater.* **2013**, *25* (33), 4653–4656.
- (32) Chen, Y.-C.; Prokleška, J.; Xu, W.-J.; Liu, J.-L.; Liu, J.; Zhang, W.-X.; Jia, J.-H.; Sechovský, V.; Tong, M.-L. A Brilliant Cryogenic Magnetic Coolant: Magnetic and Magnetocaloric Study of Ferromagnetically Coupled GdF_3 . *J. Mater. Chem. C* **2015**, *3* (47), 12206–12211.
- (33) Xu, Q.-F.; Chen, M.-T.; Wu, R.-T.; Long, L.-S.; Zheng, L.-S. Achieving Magnetic Refrigerants with Large Magnetic Entropy Changes and Low Magnetic Ordering Temperatures. *J. Am. Chem. Soc.* **2024**, *146* (29), 20116–20121.
- (34) Duval, J.-M.; Camus, P.; Calvo, M.; Prouvé, T.; Exshaw, O.; Brasiliano, D. P. Development of an ADR Refrigerator with Two Continuous Stages. *J. Low. Temp. Phys.* **2016**, *184* (3–4), 604–608.
- (35) Shirron, P. Optimization Strategies for Single-Stage, Multi-Stage and Continuous ADRs. *Cryogenics* **2014**, *62*, 140–149.
- (36) Xiang, J.; Zhang, C.; Gao, Y.; Schmidt, W.; Schmalzl, K.; Wang, C.-W.; Li, B.; Xi, N.; Liu, X.-Y.; Jin, H.; Li, G.; Shen, J.; Chen, Z.; Qi, Y.; Wan, Y.; Jin, W.; Li, W.; Sun, P.; Su, G. Giant Magnetocaloric Effect in Spin Supersolid Candidate $\text{Na}_2\text{BaCo}(\text{PO}_4)_2$. *Nature* **2024**, *625* (7994), 270–275.
- (37) Liu, X.-Y.; Gao, Y.; Li, H.; Jin, W.; Xiang, J.; Jin, H.; Chen, Z.; Li, W.; Su, G. Quantum Spin Liquid Candidate as Superior Refrigerant in Cascade Demagnetization Cooling. *Commun. Phys.* **2022**, *5* (1), 233.
- (38) Zeng, Q.; Ge, H.; Wu, M.; Ruan, S.; Li, T.; Wang, Z.; Li, J.; Ling, L.; Tong, W.; Huang, S.; Liu, A.; Zhou, J.; Xia, Z.; Sheng, J.; Wu, L.; Tian, Z. $\text{K}_3\text{RENb}_5\text{O}_{15}$ ($\text{RE} = \text{Ce}, \text{Pr}, \text{Nd}, \text{Sm}, \text{Gd}-\text{Ho}$): A Family of Quasi-One-Dimensional Spin-Chain Compounds with Large Interchain Distance. *Chem. Mater.* **2024**, *36* (6), 2867–2879.
- (39) Jesche, A.; Winterhalter-Stocker, N.; Hirschberger, F.; Bellon, A.; Bachus, S.; Tokiwa, Y.; Tsirlin, A. A.; Gegenwart, P. Adiabatic Demagnetization Cooling Well below the Magnetic Ordering Temperature in the Triangular Antiferromagnet $\text{KBaGd}(\text{BO}_3)_2$. *Phys. Rev. B* **2023**, *107* (10), No. 104402.
- (40) Arjun, U.; Ranjith, K. M.; Jesche, A.; Hirschberger, F.; Sarma, D. D.; Gegenwart, P. Adiabatic Demagnetization Refrigeration to Millikelvin Temperatures with the Distorted Square Lattice Magnet NaYbGeO_4 . *Phys. Rev. B* **2023**, *108* (22), No. 224415.